JACS
JOURNAL OF THE AMERICAN CHEMICAL SOCIETY
Article
pubs.acs.org/JACS

Polytypic Nanocrystals of Cu-Based Ternary Chalcogenides: Colloidal Synthesis and Photoelectrochemical Properties

Liang Wu,[†] Shi-You Chen,[‡] Feng-Jia Fan,[†] Tao-Tao Zhuang,[†] Chen-Min Dai,[‡] and Shu-Hong Yu*[,†]

[†]Division of Nanomaterials and Chemistry, Hefei National Laboratory for Physical Sciences at Microscale, Department of Chemistry, Hefei Science Center, CAS, CAS Center for Excellence in Nanoscience, University of Science and Technology of China, Hefei, Anhui 230026, People's Republic of China

[‡]Key Laboratory of Polar Materials and Devices (MOE), East China Normal University, Shanghai 200241, People's Republic of China

Supporting Information

ABSTRACT: Heterocrystalline polytype nanostructured semiconductors have been attracting more and more attention in recent years due to their novel structures and special interfaces. Up to now, controlled polytypic nanostructures are mostly realized in II–VI and III–V semiconductors. Herein, we report the synthesis and photoelectrochemical properties of Cu-based ternary I–III–VI_2 chalcogenide polytypic nanocrystals, with a focus on polytypic $CuInS_2$ (CIS), $CuInSe_2$ (CISe), and $CuIn(S_{0.5}Se_{0.5})_2$ alloy nanocrystals. Each obtained polytypic nanocrystal is constructed with a wurtzite hexagonal column and a zinc blende/chalcopyrite cusp, regardless of the S/Se ratio. The growth mechanisms of polytypic CIS and CISe nanocrystals have been studied by time-dependent experiments. The polytypic nanocrystals are solution-deposited on indium–tin oxide glass substrate and used as a photoelectrode, thus showing stable photoelectrochemical activity in aqueous solution. Density functional theory calculation was used to study the electronic structure and the band gap alignment. This versatile synthetic method provides a new route for synthesis of novel polytypic nanostructured semiconductors with unique properties.

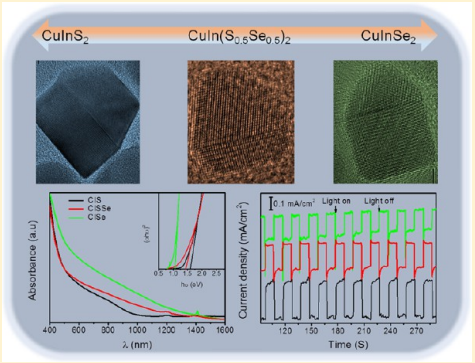

INTRODUCTION

Recently, construction of two crystal phases in single nanocrystals to form polytypic nanostructures with various shapes has been widely investigated because of their novel type of interfaces and interesting properties. These polytypic nanostructures consist of structurally different but chemically identical materials, combining harmoniously at their interfaces.[1,2] With different electronic band offset on the interface, charge carriers can be separated and accumulated in different regions, providing new possibilities to enhance the optoelectronic properties.[3,4] Polytypism widely exists in III–V and II–VI semiconductors due to their large atom stacking freedom and their phase diversity.[5−10] To date, polytypism has been reported intensively in III–V semiconductor nanowires synthesized through vapor–liquid–solid (VLS) growth[5,6,11] and II–VI semiconductor nanoarchitecture prepared by the seed-mediated solution method.[8,9,12]

The colloidal solution approach has been proven to be particularly powerful for synthesizing nanocrystals with designed structures and shapes. In particular, it is a versatile method to prepare stand heteronanostructures[13,14] and branched polytypic nanostructures.[15−17] To date, several Cu-based ternary and quaternary polytypic chalcogenide nanocrystals constructed with wurtzite and zinc blende phases have been realized by the colloidal solution approach, such as linearly arranged polytypic $Cu_2ZnSn(S_{1-x}Se_x)_4$, $Cu_2CdSn(S_{1-x}Se_x)_4$, Cu_2SnSe_3, and Cu_2GeSe_3 nanocrystals[18−22] and tetrapod-shaped Cu_2SnSe_3 and $Cu_2CdSnSe_4$ nanocrystals.[15,16,21] Cu-based ternary I–III–VI_2 semiconductors have received great interests in photovoltaic applications due to their composition-dependent band gaps, low toxicity, and high absorption coefficients.[23−26] Chalcopyrite is one common crystal structure of I–III–VI_2 semiconductors with I and III ions ordering in the anion sublattice sites. The chalcopyrite structure can be transformed to zinc blende phase through disordering the cation occupations. Another ordered phase of I–III–VI_2 has orthorhombic structure, and the disordering arrangement of cations leads to the wurtzite structure.[27−29] Structure- and shape-controlled I–III–VI_2 ternary nanocrystals have been widely reported and used in photovoltaic, photoelectrochemical, and photocatalytic areas.[30−34] Furthermore, construction of wurtzite/orthorhombic and chalcopyrite/zinc blende I–III–VI_2 in single nanocrystals to form polytypic interfaces to enhance the optoelectronic properties still remains a challenge.

In this contribution, we reported a facile colloidal method for synthesizing polytypic $CuInS_2$ (CIS), $CuInSe_2$ (CISe), and $CuIn(S_{0.5}Se_{0.5})_2$ (CISSe) alloy nanocrystals with zinc blende or chalcopyrite structure selectively growing on wurtzite structure to form bullet-shaped polytypic nanostructures. Similar to

Received: December 20, 2015
Published: April 11, 2016

DOI: 10.1021/jacs.5b13288
J. Am. Chem. Soc. 2016, 138, 5576−5584

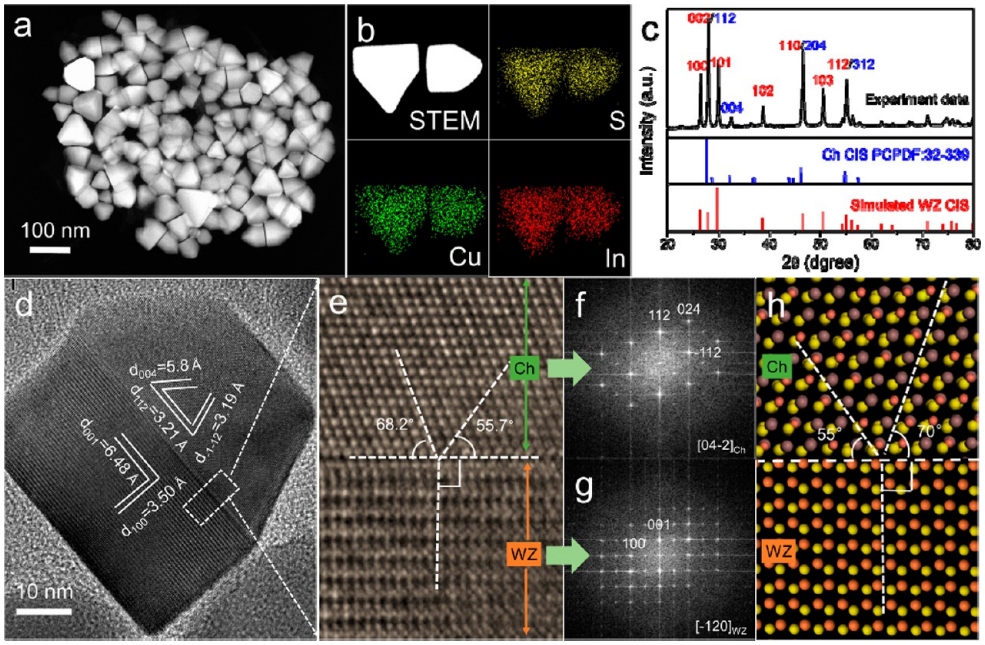

Figure 1. (a) HAADF-STEM image of the polytypic CIS nanocrystals. (b) EDS mapping of two randomly selected polytypic CIS nanocrystals. (c) XRD pattern. For reference, the chalcopyrite and simulated wurtzite XRD patterns of CIS are shown below. (d) HRTEM image. (e) The enlarged HRTEM image of the selected area in part d. (f, g) FFT images of different areas in the HRTEM image. (h) The crystal model of the interface of the wurtzite and chalcopyrite structures. The yellow spheres refer to S atoms. The purple spheres refer to In atoms. The orange spheres refer to Cu/In atoms. The red spheres refer to the Cu atoms.

wurtzite CdSe nanostructures, wurtzite CIS(Se) has two exposed facets, (002) and (00$\bar{2}$), which can serve as nucleated substrates for epitaxial growth of other nanocrystals. So two $\{002\}_{WZ}$ facets can serve as nucleation facets for epitaxial growth of chalcopyrite or zinc blende structure because the $\{002\}_{WZ}$ facets can interface with $\{111\}_{ZB}$ and $\{112\}_{Ch}$ facets due to the low lattice mismatch. The polytypic characteristic of the obtained nanocrystals was confirmed by transmission electron microscopy (TEM) and X-ray power diffraction (XRD) analysis. Time-dependent experiments have studied the growth process of polytypic CIS and CISe nanocrystals, respectively. Moreover, we investigated the optical properties of the obtained polytypic nanocrystal and the photoelectrochemical properties of their thin films prepared through dip-coating polytypic nanocrystals on indium−tin oxide (ITO) glass.

EXPERIMENTAL SECTION

Materials. Ethanol (99.7%), hexane (97%), 1-dodecanethiol (97%, DDT), tetrachloroethylene (98.5%), CuI (97%), $In(NO_3)_3{\cdot}xH_2O$ (99.5%), SeO_2 (99.9%), Se powder (99.95%), S powder (99.5%), chloroform, and Na_2SO_4 (99.9%) were purchased from Sinopharm Chemical Reagent Co. Ltd. (Shanghai, China). $InCl_3$ (99.9%) was purchased from Alfa Aesar. Oleylamine (80%−90%) was purchased from Aladdin Reagent Co. Ltd. (Shanghai, China). Diphenyl disenenide (99%) was purchased from Acros Organics. All chemical reagents were used as received without further purification.

Synthesis of Polytypic CIS Nanocrystals. In a typical synthsis, stoichiometric amounts of CuI (0.2 mmol) and $InCl_3$ (0.2 mmol) were dissolved in 10 mL of oleylamine with the presence of 1 mL of 1-dodecanethiol in a three-necked flask in air, and then the mixture was heated up to 280 °C at a heating rate of 10 °C/min and kept at 280 °C for 60 min. The flask was removed from the heating mantle and naturally cooled down. The black product was collected and centrifuged at 8000 rpm for 5 min, and the upper clear solution was discarded. Then hexane was added to disperse the nanocrystals. To collect the nanocrystals again, ethanol was added into the dispersion and the formed slurry was centrifuged again at 8000 rpm for 5 min. The nanocrystals were washed by repeating the above dispersing and depositing process two times.

Synthesis of Polytypic CISe Nanocrystals. Typically, stoichiometric amounts of CuI (0.2 mmol) and $In(NO_3)_3{\cdot}xH_2O$ (0.2 mmol) were dissolved in 8 mL of oleylamine in the presence of 300 μL of 1-dodecanethiol in a three-necked flask in air, and then the mixture was heated up to 180 °C. At the same while, 0.8 mmol of diphenyl diselenide was dissolved in another three-necked flask containing 3 mL of oleylamine in air at 70 °C. The reaction solutions were mixed by injecting the diphenyl diselenide solution into the former salt solution. The temperature of the reaction solution was increased from 150 to 280 °C at a heating rate of 10 °C/min and kept at 280 °C for 30 min. The product was collected and washed using the same procedure as for polytypic CIS.

Synthesis of Polytypic CISSe Nanocrystals. The synthesis method is the same as that for CISe polytypic nanocrystals with the replacement of 300 μL of 1-dodecanethiol with 1 mL and of 0.8 mmol of diphenyl diselenide with 0.2 mmol.

Preparation of Thin Films of Polytypic Nanocrystals. The polytypic nanocrystal thin film electrodes were prepared by dip-coating their colloidal ink over ITO glass, and the electrodes were annealed in vacuum for 12 h at 150 °C to remove the organic ligands.

Characterization. The specimen prepared by drop-casting on a Si substrate was characterized by powder X-ray power diffraction (PXRD), using a Philips X'Pert PRO SUPER X-ray diffractometer equipped with graphite-monochromatized Cu Kα radiation (λ = 1.54 056 Å). The operation voltage and current were kept at 40 kV and 400 mA, respectively. The simulated wurtzite CIS, CISSe, and CISe powder XRD patterns were obtained from Diamond 3.2. Nanocrystals dispersed in hexane were dropped on a Mo grid for TEM, high-resolution transmission electron microscopy (HRTEM), and high-angle annular dark field (HAADF) investigation, which were performed on JEOL-2010F and JEM-ARM200F instruments with an acceleration voltage of 200 kV. Energy dispersive spectrometry (EDS) was carried out on an Inca Oxford equipped on the JEOL-2010F. Raman spectra were recorded with a Renishaw System 2000 spectrometer using the 514 nm line of semiconductor lasers for excitation. UV−vis−NIR spectroscopy of the polytypic nanocrystals

DOI: 10.1021/jacs.5b13288
J. Am. Chem. Soc. 2016, 138, 5576−5584

dispersed in tetrachloroethylene were measured at room temperature using a DUV-3700 UV−vis−NIR spectrometer (Shimadzu). XPS was performed on an ESCALab MKII X-ray photoelectron spectrometer using a Mg Ka radiation exciting source.

Photoelectrochemical Measurement. The electrochemical measurements were performed in a three-electrode cell with a Ag/AgCl electrode as a reference electrode and a platinum wire as a counter electrode. The active area of the electrode was 2 cm^2. All measurements were carried out in an aqueous solution of 0.2 M Na_2SO_4 electrolyte. Photocurrent was detected with a scanning potentiostat (CH Instruments, model CHI 760E) under chopped irradiation from a 150 W Xe lamp equipped with an AM1.5 filter.

RESULTS AND DISSCUSION

Polytypic CIS, CISe, and CISSe Nanocrystals. For CIS, wurtzite is a metastable structure derived from wurtzite ZnS through random substitution of Zn atoms with Cu and In atoms. Wurtzite CIS synthesized by using a proper sulfur source (such as DDT, HDT) widely exists in nanostructure but not in bulk,[23,27,35,36] while the chalcopyrite structure, which is the stable phase of CIS, can be formed at high temperature.[37] If DDT is used as the sulfur source for synthesizing CIS nanocrystals at high temperature, the metastable wurtzite and stable chalcopyrite phase would coexist in single nanocrystals to form polytypic structures. When DDT was substituted by S powder, the CIS crystallized into chalcopyrite structure [Figure S1, Supporting Information (SI)]. If $InCl_3$ is substituted by $In(NO_3)_3{\cdot}xH_2O$, irregular CIS nanocrystals were obtained (Figure S2, SI).[38] TEM and HAADF-STEM images [Figure S3a,b (SI) and Figure 1a] show the obtained bullet-shaped polytypic CIS nanocrystals. EDS mapping of the randomly selected CIS nanocrystals (Figure 1b) illustrates that Cu, In, and S elements distribute homogeneously in the bullet-shaped nanocrystals with a mole ratio of 1/0.9/1.9 and no noticeable nanoheterostructure can be observed in the mapping. The structure of the prepared nanocrystals was characterized by power X-ray diffraction (PXRD), as shown in Figure 1c. The main peaks at 26.3°, 27.9°, 29.9°, 38.7°, 46.5°, 50.6°, and 55.1° can be indexed to the (100), (002), (101), (102), (110), (103), and (112) planes of wurtzite CIS. As the (002), (110), and (112) planes of wurtzite CIS overlap with the (112), (204) and (312) planes of chalcopyrite CIS, the stronger diffraction of those peaks as well as the peak at 32.4°, which can be indexed to the (004) plane of chalcopyrite CIS (Figure S4, SI), confirms the coexistence of chalcopyrite structure.

HRTEM images and the corresponding fast Fourier transform (FFT) images are shown in Figure 1d−g for further studying of the structure of the obtained CIS nanocrystals. There are two distinct parts (rectangle and trapezold areas) in the CIS nanocrystals. In the rectangle area, the observed two vertical planes with *d*-spacing of 3.50 and 6.48 Å can be indexed to the (110) and (001) planes of wurtzite CIS. The observed *d*-spacing of 3.19, 3.21, and 5.80 Å in the trapezoid region correspond to the $(\bar{1}\bar{1}2)$, (112), and (004) planes of chalcopyrite CIS. The FFT images (Figure 1f,g) of the selected areas also testify to the wurtzite structure of rectangle part and chalcopyrite structure of trapezoid part, respectively. A magnified HRTEM image (Figure 1e) and the corresponding crystal model (Figure 1h) show the interface of the two structures, where we can observe the arrangement of atoms.

Similar to CIS, CISe has two different structures: the stable zinc blende and the metastable wurtzite. Note that the metastable wurtzite CISe nanocrystals can be synthesized by using diorgano diselenide as selenium source at a proper reaction temperature.[24,31,39,40] It is observed that interesting novel nanoheterostructured CISe nanocrystals could be obtained by using diphenyl disenenide as selenium source at high reaction temperature. Zinc blende CISe nanocrystals would be obtained under the same reaction conditions (Figures S5 and S6, SI) with SeO_2 and Se.[41,42] The HAADF-STEM and TEM images of the nanocrystals synthesized at 280 °C in Figure 2a and Figure S3c,d (SI) revealed that the CISe

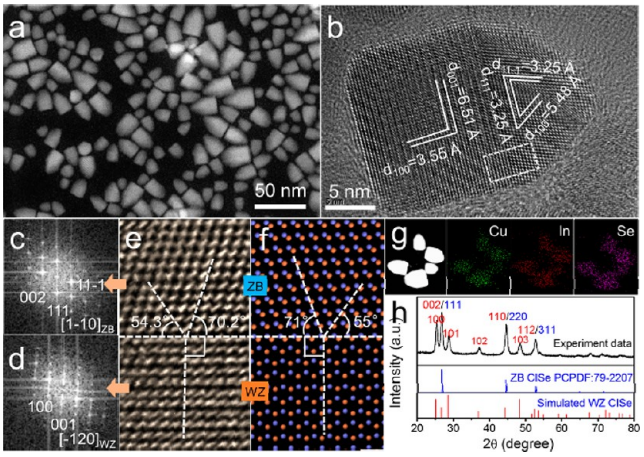

Figure 2. (a, b) HAADF-STEM and HRTEM images of polytypic CISe nanocrystals. (c, d) FFT images of different areas in the HRTEM image. (e) The enlarged HRTEM image in the selected area in part b. (f) The crystal model of the interface of wurtzite and zinc blende structures. The blue spheres refer to Se atoms, and the orange spheres refer to Cu/In atoms. (g) EDS mapping of the randomly selected polytypic CISe nanocrystals. (h) XRD pattern. For reference, the zinc blende and simulated wurtzite XRD patterns of CISe are shown below.

nanocrystals possessed bullet shape with an average long and short diameter of 17.5 and 11.4 nm. The HRTEM images (Figure 2b,e) and FFT images (Figure 2c,d) illustrate the detailed structure information on the bullet-shaped nanocrystals. The *d*-spacing of 6.51 and 3.55 Å in the rectangle area can be indexed to the (001) and (100) planes of wurtzite CISe and the *d*-spacing of 3.25, 3.25, and 5.48 Å in the cusp area agree with the $(1\bar{1}1)$, (111), and (100) planes of zinc blende CISe. The crystal model shown in Figure 2f exhibits the interface of the wurtzite and zinc blende structures.

Note also that the contrast difference of the synthesized nanocrystals is obviously observed in the TEM images (Figure S3c,d, SI). As we known, the contrast difference observed in nanoheterostructures is attributed to the different mass thickness and diffraction. In order to clarify whether the contrast difference comes from the composition variation or not, STEM-EDS element mapping was recorded (Figure 2g), and it confirmed that Cu, In, and Se elements distribute homogeneously in the randomly selected polytypic nanocrystals. The structure of the polytypic CISe nanocrystals was further characterized by PXRD (Figure 2h). The zinc blende and simulated wurtzite diffraction patterns are also showed in Figure 2h for reference. The PXRD patterns of polytypic CISe are similar to those of the polytypic CIS nanocrystals, and all peaks can be indexed to the crystal facets of simulated wurtzite CISe, while the peaks shared with the zinc blende structure are intensified due to the coexistence of the zinc blende structure. It should be noted that DDT was necessary for the systhesis of polytypic CISe nanocrystals, even though the DDT might react

DOI: 10.1021/jacs.5b13288
J. Am. Chem. Soc. 2016, 138, 5576−5584

with Cu and In precursors. Irregular CISe nanocrystals are obtained in the absence of DDT under the same reaction conditions (Figure S7, SI). The DDT was used as ligands to keep the shape of the obtained nanocrystals. In order to impede the DDT from participating in the reaction, 4 times the selenium source was added to the reaction. The EDS spectrum in Figure S14d (SI) indicated that the obtained polytypic nanocrystals contained sulfur.

For compound semiconductor, forming mixed-anion alloys is an important way to tune their photoelectric properties. For example, the efficiency of a $Cu_2ZnSn(S_{1-x}Se_x)_4$ solar cell is higher than that of pure Cu_2ZnSnS_4 and $Cu_2ZnSnSe_4$ solar cells.[43−45] It should be noted that alloy $CuIn(S_{1-x}Se_x)_2$ nanocrystals with pure phase have been synthesized;[46,47] however, the polytypic $CuIn(S_{1-x}Se_x)_2$ alloy nanocrystals have been rarely reported. Figure 3a shows the polytypic CISSe

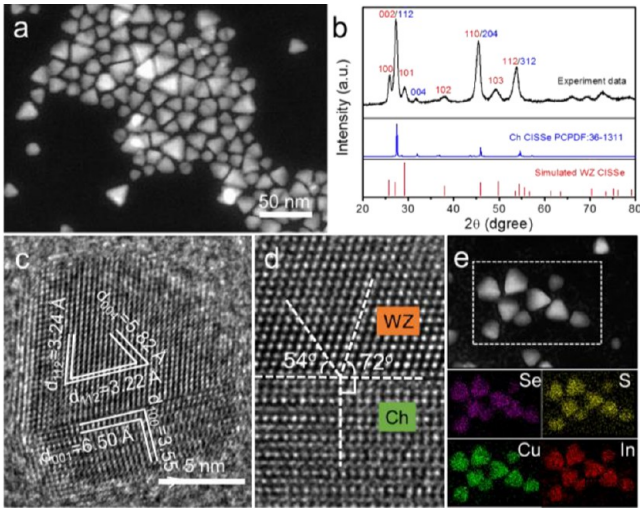

Figure 3. (a) HADDF-STEM image of the polytypic CISSe alloy nanocrystals. (b) XRD patterns of the polytypic CISSe alloy nanocrystals. For reference, the chalcopyrite and simulated XRD patterns of CISSe are shown below. (c, d) HRTEM and enlarged HRTEM images of the polytypic CISSe nanocrystals. (e) STEM-EDS element mapping of the randomly selected polytypic CISSe nanocrystals.

nanocrystals synthesized with a proper ratio of 1-DDT and diphenyl diselenide (Table S1, SI). The XRD result shown in Figure 3b is similar to the XRD patterns of polytypic CIS and CISe nanocrystals, indicating the coexistence of wurtzite and chalcopyrite structures. The peaks at 27.4°, 45.7°, and 54.1° with enhanced intensity are attributed to the overlapping of the wurtzite and chalcopyrite peaks. The HRTEM images shown in Figure 3c,d further confirm the polytypic alloy nanocrystals. In accordance with the TEM image, the nanocrystals can be divided into two distinct domains: the chalcopyrite triangle domain and the wurtzite rectangle domain. In order to exclude that the heterostructures are formed via maldistribution of the elements, EDS element mapping is carried out. The result illustrates that the Cu, In, S, and Se elements with mole ratio of 1/1/1/1 distribute homogeneously in the polytypic nanocrystals, indicating no heterostructure formation in the nanocrystals. Other polytypic CISSe alloy nanocrystals with different S/Se ratio can be synthesized through changing the ratio of 1-DDT and diphenyl diselenide under the same reaction conditions (Table S1, SI). Figures S8 and S9 (SI) show the TEM images, XRD patterns, and EDS spectra of polytypic $CuIn(S_{0.3}Se_{0.7})_2$ and $CuIn(S_{0.7}Se_{0.3})_2$ nanocrystals, respectively.

According to the statistical data from the TEM images, the yields of the polytypic CIS, CISe, and CISSe nanocrystals are 85%, 84%, and 90%, respectively. We attribute the observation of odd shapes in Figure S3 (SI), e.g. spherical shape, to the viewing angle of the nanocrystal. They are bullet-like in shape with their vertical axis along the [001] direction. Viewing from this direction, they are round in shape. A lack of uniformity in sizes can be attributed to the high growth temperature and long reaction time. However, since the quantum confinement effect is absent in these nanocrystals, it has negligible impact on the band gaps and therefore the photoelectrochemical properties.

Absorption spectra were used to research the optical properties of the obtained polytypic nanocrystals. As shown in Figure 4a, the three different polytypic nanocrystals show

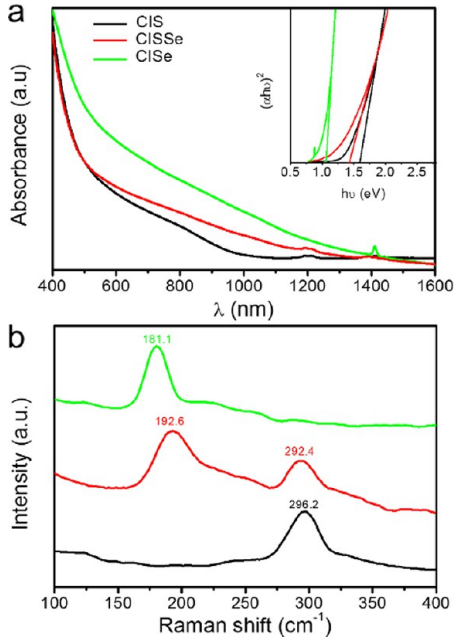

Figure 4. (a) Absorption spectra of the synthesized polytypic nanocrystals, which are dispersed in tetrachloroethylene. The inset shows the linear extrapolation of $(\alpha h\upsilon)^2$ versus photon energy $(h\upsilon)$. (b) Room temperature Raman spectra of the synthesized polytypic nanocrystals with a 514 nm laser.

significant absorption in the visible spectral region. The optical band gaps were estimated through extrapolating the linear region of the plot of $(\alpha h\upsilon)^2$ versus photon energy $(h\upsilon)$ (the inset in Figure 4a). The results of 1.12, 1.45, and 1.52 eV, which belong to the polytypic CISe, CISSe and CIS nanocrystals, respectively, are similar to the reported band gaps of the tetragonal $CuIn(S_{1-x}Se_x)_2$ nanocrystals with the same chemical composition and change according to the S/Se ratio.[46] Lower energy shoulders of the absorption spectra marked the similar band gaps.[48]

Room temperature Raman spectra were used to further study the structure of the obtained polytypic nanocrystals because the XRD pattern cannot accurately distinguish the binary $Cu_2S(Se)$ and $CuInS(Se)_2$. The wurtzite CIS and CISe show Raman spectra similar to those of chalcopyrite and zinc blende CIS and CISe, like wurtzite CZTS and CZTSe show Raman spectra similar to those of zinc blende CZTS and CZTSe.[49] The peaks at 181.1 and 296.2 cm^{-1} (Figure 4b) for polytypic CIS and

DOI: 10.1021/jacs.5b13288
J. Am. Chem. Soc. 2016, 138, 5576−5584

CISe almost match the intense peaks of the reported CIS and CISe,[50,51] respectively, where the shift of the peaks can be due to the defect and size effect.[52,53] The presence of single peaks confirms the formation of ternary naoncrystals and there is no presence of binary nanocrystals. The Raman spectra of the alloyed polytypic nanocrystals exhibit two-mode behaviors (one CISe-like mode at 192.6 cm^{-1} and another CIS-like mode at 292.4 cm^{-1}). This similar two-mode behavior has been found in the reported CZTSSe.[54] Both of the modes have a little shift due to the effect of the chalcogen ratio.[41] There is no CIS-like mode in the Raman spectra of polytypic CISe nanocrystals, illustrating that the DDT almost does not participate in the reaction and acts as ligand, as well as that the sulfur on the polytypic CISe probably comes from the DDT ligands.

X-ray photoelectron spectroscopy (XPS) analysis was used to investigate the oxidation state of the surface elements of the obtained nanocrystals. The two characteristic Cu_{2p} peaks of the obtained three nanocrystals, which all located at 932.2 and 952 eV with a binding energy splitting of 19.8 eV, indicate the presence of the Cu(I) state (Figure S10a, SI). The In of the three nanocrystals has the same 3d peaks located at 444.5 and 452 eV with a binding splitting of 7.5 eV, indicating the presence of the In(III) state (Figure S10b, SI). Then, the Se_{3d} peaks of polytypic CISSe and CISe appear at 53.5 and 54.6 eV, confirming the presence of the Se(II) state (Figure S10c, SI), and the typical S_{2p} peaks of CIS and CISSe at 161.9 and 163 eV can be index to the peaks of the S(II) state (Figure S10d, SI). Thus, the results of XPS analysis indicate that the phase and composition cannot influence the element oxidation state of the obtained nanocrystals.

Growth Mechanism of Polytypic CIS and CISe Nanocrystals. These Cu-based polytypic ternary nanocrystals can be synthesized through a simple colloidal method, while the growth process of these polytypic nanocrystals is still an open question. In our previous work, we have reported that the polytypic $Cu_2ZnSn(S_xSe_{1-x})_4$ nanocrystals could be obtained through subsequent epitaxial growth of zinc blende structure on the wurtzite structure nucleated at low temperature.[18] According to the growth mechanism study of polytypic $Cu_2ZnSn(S_xSe_{1-x})_4$, time-dependent experiments were performed to show the growth process of polytypic CIS and CISe nanocrystals. On the basis of the color change of the reaction solution for polytypic CIS synthesis, the nanocrystals nucleated at 240 °C, and an aliquot was taken when the reaction temperature increased to 260 °C. The aliquot was characterized by TEM, HRTEM, EDS, and PXRD. Figure 5 shows the TEM and HRTEM images of the aliquots taken during the polytypic CIS synthesis process. First, nanoparticles of ca. 6 nm diameter were obtained when the reaction temperature reached 260 °C (Figure 5a,b). The PXRD patterns (Figure S11, SI) can be indexed to $Cu_{31}S_{16}$ (PCPDF: 23-959) and the lattice spacing of 3.42 Å (Figure 5b) agrees with the identity distance of the (004) plane of $Cu_{31}S_{16}$. It illustrates that the DDT first reacts with Cu precursor to form $Cu_{31}S_{16}$ nanocrystals at low temperature. The EDS spectrum also indicates the existence of $Cu_{31}S_{16}$ (Figure S12a, SI). Then, nanocylinders were obtained when the reaction solution was kept at 280 °C for 5 min. The planes with lattice spacing of 3.51 Å (Figure 5d) and 6.51 Å (Figure 5e) are indexed to the (100) and (001) planes of wurtzite CIS, respectively. The PXRD patterns shown in Figure S11 (SI) further prove the wurtzite structure of the nanocylinders, and the EDS spectrum (Figure S12b, SI) illustrates the existence of Cu, In, and S with a mole ratio of 1/0.3/1. Lately, ladder-shaped nanocrystals (Figure 5f) were obtained when the reaction solution was kept at 280 °C for 15 min. The HRTEM image (Figure 5g) shows two different regions that can be indexed to wurtzite and chalcopyrite CIS, and the PXRD patterns (Figure S11, SI) also prove the coexistence of wurtizte and chalcopyrite phases. The EDS spectrum (Figure S12c, SI) shows that the mole ratio of Cu/In/S increases to 1/0.5/1.8. After reacting at 280 °C for 60 min, bullet-shaped polytypic CIS nanocrystals with a mole ratio of 1/0.9/1.9 were obtained (Figure S12d, SI). The time-dependent experiments provided the growth process information on polytypic CIS nanocrystals. First, the $Cu_{31}S_{16}$ nanocrystals nucleate at low temperature, followed by diffusion of In ions into $Cu_{31}S_{16}$ nanocrystals to form wurtzite CIS nanocylinders, and then chalcopyrite CIS nucleates on the (001) facet of wurtzite CIS to form a bullet-shaped polytypic nanocrystals (Scheme 1a). However, the growth mechanism of polytypic CISe nanocrystals is different from that of the polytypic CIS nanocrystals (Scheme 1b). According to the color change of the reaction solution, we found the reaction started at a low temperature of 220 °C. Wurtzite CISe nanoparticles with a mole ratio of 1/0.6/1.1 were obtained when the reaction temperature increased to 240 °C [Figure 6a,b and Figures S13 and S14 (SI)]. Then, wurzite CISe nanoparticles would grow into wurtzite hexagonal prisms with a

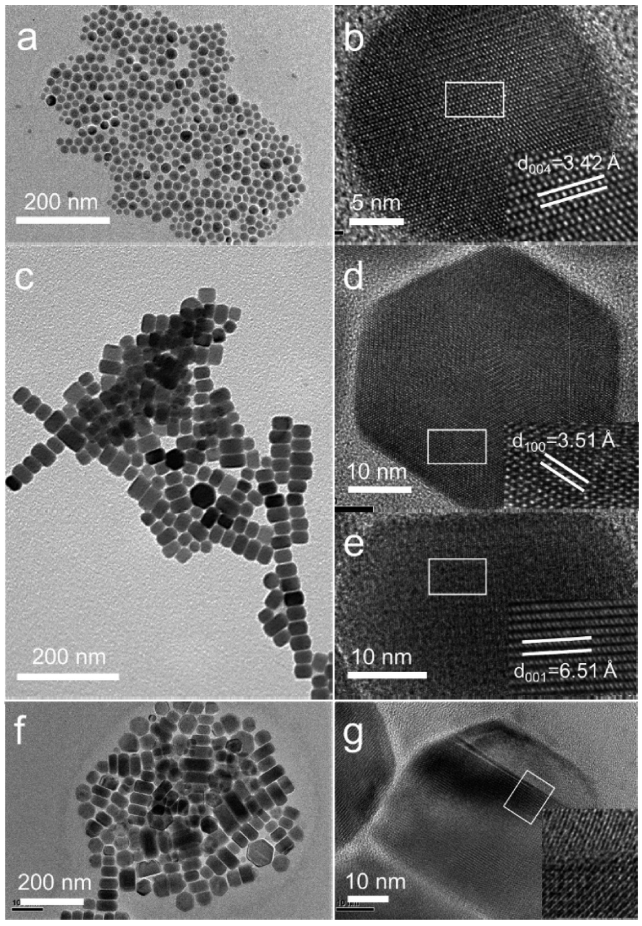

Figure 5. TEM and HRTEM images of nanocrystals prepared at different stages of the synthesis process of the polytypic CIS nanocrystals: (a, b) the reaction temperature reached 260 °C, (c–e) the reaction was kept at 280 °C for 5 min, and (f, g) the reaction was kept at 280 °C for 15 min.

DOI: 10.1021/jacs.5b13288
J. Am. Chem. Soc. 2016, 138, 5576–5584

Scheme 1. Schematic Illustration of the Growth Mechanisms of (a) Polytypic CIS and (b) Polytypic CISe Nanocrystals

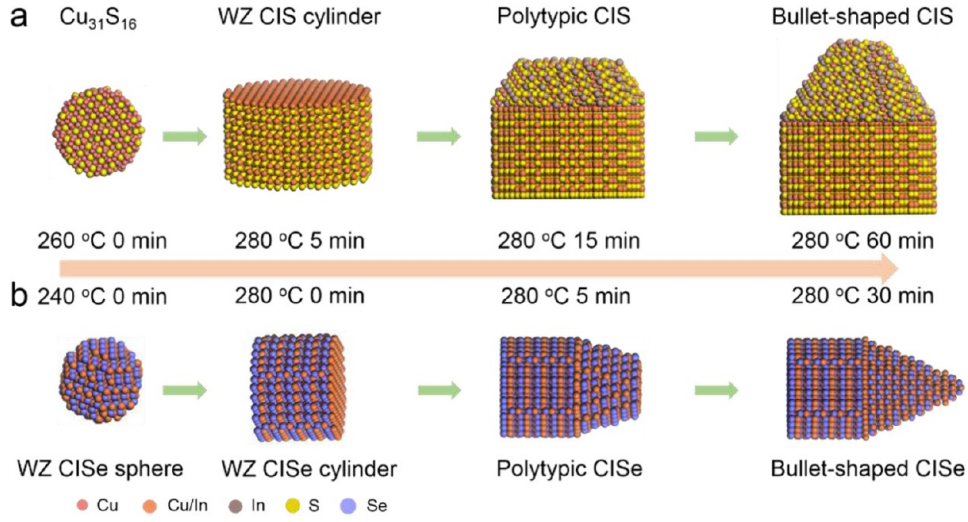

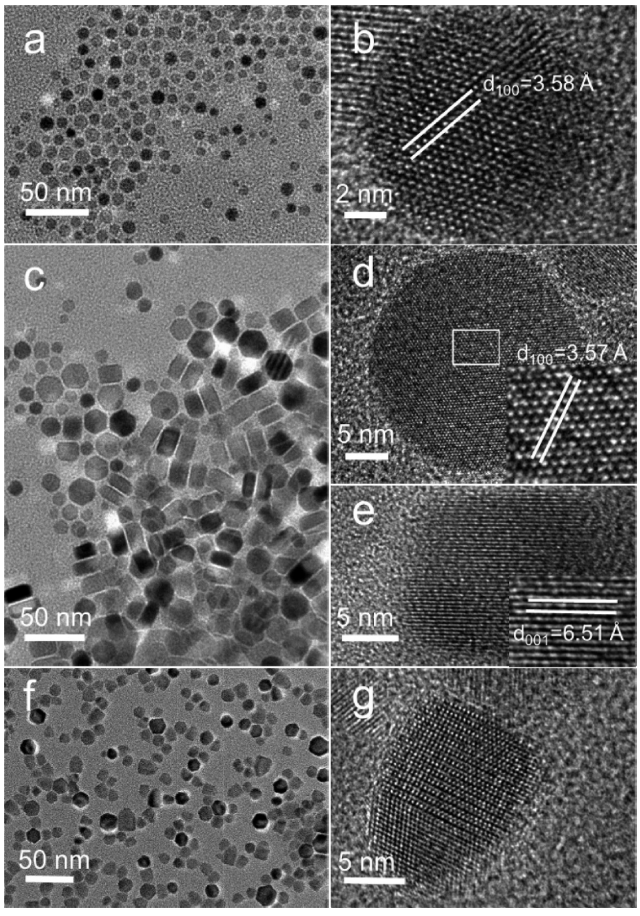

Figure 6. TEM and HRTEM images of the nanocrystals obtained at the different stages of the synthesis process of polytypic CISe nanocrystals: (a, b) the reaction temperature reached at 240 °C, (c–e) the reaction temperature arrived at 280 °C, and (f, g) the reaction was kept at 280 °C for 5 min.

mole ratio of 1/0.6/1.2 [Figure 6c–e and Figures S13 and S14 (SI)]. Lately, zinc blende CISe selectively grew on wurtzite hexagonal prisms to form polytypic nanocrystals after keeping the reaction temperature at 280 °C for 5 min [Figure 6f,g and Figures S13 and S14 (SI)]. The slight diversity of the growth mechanism between CIS and CISe polytypic nanocrystals can be attributed to the different reactivity of DDT and diphenyl disenenide.

Photoelectrochemical Properties. Recently, I–III–VI ternary nanocrystals have been suggested as promising materials for fabrication of solar cell and photocatalyst for solar hydrogen production.[33,34,55–58] In order to demonstrate the potential applications of these ternary polytypic nanocrystals in solar harvesting, the photocurrent density–time response of the polytypic nanocrystal films was invested in a photoelectrochemical cell (PEC) containing 0.2 M Na_2SO_4(Figure 7a). The polytypic nanocrystals produce a cathodic photocurrent that increases gradually with increasing negative potential (Figure S15, SI), which indicates that the polytypic nanocrystal films behaved as a p-type semiconductor photoelectrode. The transient photocurrent generated from the as-deposited polytypic nanocrystal thin films was observed at a constant potential of −0.6 V (vs Ag/AgCl) at the light-on and light-off time of 10 s (Figure 7b). The polytypic CIS film shows a constant photocurrent density of 0.29 mA/cm^{-2}, which remained over several cycles, as well as a stable photocurrent and a dark current, and the constant photocurrent density of CISSe and CISe films are 0.21 and 0.19 mA/cm^{-2}, respectively. The CISSe film shows a little current drop under illumination, while the CISe film exhibits an obvious current drop. The current drop is due to the decomposition of the selenide on the electrode.

To understand the good PEC activity of the polytypic nanocrystals, we calculated the electronic band offset between the wurtzite and chalcopyrite phases of CIS. A coherent interface can be formed between the (112) surface of the chalcopyrite structure and the (002) surface of the wurtzite structure, without dangling or wrong bonds. This makes the calculation of the band offset between the two phases in the polytypic nanocrystals possible. The calculation details are given in previous reports,[41,59] and the results are plotted in Figure 8.

When the phases form a periodic superlattice along the wurtzite [002] (or chalcopyrite [112]) direction, all the interfaces are coherent, so the electronic band structure of the superlattice is very similar to that of the isolated wurtzite or chalcopyrite phases, as shown by the calculated density of states in Figure 8b. A type II band alignment can be derived, with the

DOI: 10.1021/jacs.5b13288
J. Am. Chem. Soc. 2016, 138, 5576–5584

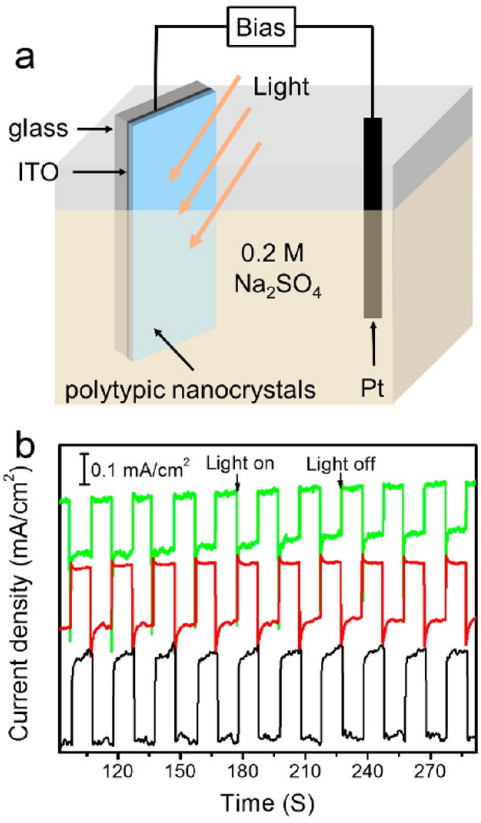

Figure 7. (a) Schematic representation of PEC with polytypic nanocrystals on ITO and commercial Pt film as photocathode and photoanode, respectively. (b) The photocurrent density−time response of the polytypic CIS (black), CISSe (red), and CISe (green) nanocrystal films at a potential of −0.6 V.

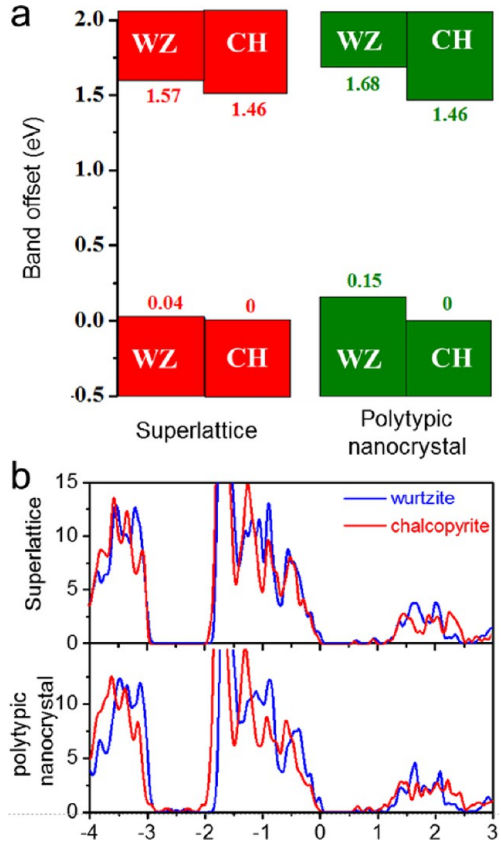

Figure 8. (a) The calculated band alignment between the wurtzite and chalcopyrite phases of CIS and (b) the calculated density of states of the two phases, in two different configurations: the superlattice with wurtzite/chalcopyrite phases repeated periodically along the [002] (or [112]) direction, and the polytypic nanocrystal with one interface formed between the two phases and two passivated surfaces at the bottom and top, respectively. The latter is similar to the synthesized polytypic nanocrystals.

valence (conduction) band edge of the wurtzite phase slightly higher than that of the chalcopyrite phase, as shown in Figure 8a. Therefore, the photogenerated electron−hole pairs can be separated in the superlattice. However, since the band offsets are small, this separation is slow, which well limits the PEC performance.

When the two phases form the polytypic nanocrystals (as we synthesized), a coherent interface is formed, and meanwhile, two surfaces are formed at the two ends of the nanocrystals. Our calculations showed that the two ending surfaces could be passivated through forming sulfur vacancies on the sulfur-terminated surfaces and forming Cu vacancies on the cation-terminated surfaces. In the polytypic nanocrystals, the calculated band alignment is still type II, but the band offsets are obviously larger, so an obvious upward shift can be found in the density of states of the wurtzite phase relative to the chalcopyrite phases. This indicates that the photogenerated electron−hole pairs can be separated more efficiently, which can explain our observed PEC activity enhancement. In contrast with the periodic superlattice, the polytypic nanocrystals have a much lower symmetry, which makes the electrostatic potential difference between the two phases much larger, thus increasing the band offsets. Since the low symmetry is general for all the polytypic nanocrystals, independent of the specific surface passivation or the shape of the nanocrystals, we can expect that the PEC activity enhancement is also general, which is an intrinsic properties of the polytypic nanocrystals.

CONCLUSION

In summary, a facile colloidal method for synthesis of Cu-based ternary polytypic nanocrystals with zinc blende or chalcopyrite structure selectively growing on wurtzite structure has been reported. The obtained nanocrystals with bullet-shape have a wurtzite hexagonal column and a zinc blende/chalcopyrite cusp, regardless of the S/Se ratio. Time-dependent experiments indicate that the polytypic CIS and CISe have different growth mechanisms. In the synthesis of polytypic CIS, $Cu_{31}S_{16}$ nanocrystals first nucleated at low temperature, the In ions then inserted into the $Cu_{31}S_{16}$ nanocrystals to form CIS nanocylinders, and, finally, chalcopyrite CIS nucleated on the (001) facet of wurtzite CIS to form bullet-shaped polytypic nanocrystals. In the synthesis of CISe, the wurzite CISe nanoparicle nucleated at low temperature and grew into wurtzite hexagonal prims under increasing temperature, and, last, zinc blende CISe selectively grew on one facet of the wurtzite hexagonal prims to form bullet-shaped nanocrystal. Indeed, preliminary experiments show that the films prepared from polytypic nanocrystal solution-deposited on ITO glass show good photoelectrochemical activity in aqueous solution. DFT calculations shows that the band alignment of the polytypic nanocrystals is type II, which is beneficial for separation of photogenerated electron−hole pairs and leads to a good PEC performance. These special polytypic ternary

DOI: 10.1021/jacs.5b13288
J. Am. Chem. Soc. 2016, 138, 5576−5584

nanocrystals may find potential applications in energy conversion and photocatalysis in the future.

■ ASSOCIATED CONTENT

Supporting Information

The Supporting Information is available free of charge on the ACS Publications website at DOI: 10.1021/jacs.5b13288.

Crystal data for CIS, CISe, CISSe; Table S1; and Figures S1− S15 (PDF)

■ AUTHOR INFORMATION

Corresponding Author

*shyu@ustc.edu.cn

Author Contributions

L.W. and S.-Y.C. contributed equally. The manuscript was written through contributions of all authors. All authors have given approval to the final version of the manuscript.

Notes

The authors declare no competing financial interest.

■ ACKNOWLEDGMENTS

S.H.Y. acknowledges the funding support from the National Natural Science Foundation of China (Grants 21431006), the Foundation for Innovative Research Groups of the National Natural Science Foundation of China (Grant 21521001), the National Basic Research Program of China (Grants 2014CB931800, 2013CB933900), and the Users with Excellence and Scientific Research Grant of Hefei Science Center of CAS (2015HSC-UE007, 2015SRG-HSC038).

■ REFERENCES

(1) Li, L.; Gan, Z.; McCartney, M. R.; Liang, H.; Yu, H.; Yin, W.-J.; Yan, Y.; Gao, Y.; Wang, J.; Smith, D. J. *Adv. Mater.* **2014**, *26*, 1052.

(2) Bechstedt, F.; Käckell, P. *Phys. Rev. Lett.* **1995**, *75*, 2180.

(3) Liu, M.; Jing, D.; Zhou, Z.; Guo, L. *Nat. Commun.* **2013**, *4*, 2278.

(4) Scanlon, D. O.; Dunnill, C. W.; Buckeridge, J.; Shevlin, S. A.; Logsdail, A. J.; Woodley, S. M.; Catlow, C. R. A.; Powell, M. J.; Palgrave, R. G.; Parkin, I. P.; Watson, G. W.; Keal, T. W.; Sherwood, P.; Walsh, A.; Sokol, A. A. *Nat. Mater.* **2013**, *12*, 798.

(5) Caroff, P.; Dick, K. A.; Johansson, J.; Messing, M. E.; Deppert, K.; Samuelson, L. *Nat. Nanotechnol.* **2009**, *4*, 50.

(6) Vainorius, N.; Lehmann, S.; Jacobsson, D.; Samuelson, L.; Dick, K. A.; Pistol, M. E. *Nano Lett.* **2015**, *15*, 2652.

(7) Li, H.; Kanaras, A. G.; Manna, L. *Acc. Chem. Res.* **2013**, *46*, 1387.

(8) Milliron, D. J.; Hughes, S. M.; Cui, Y.; Manna, L.; Li, J.; Wang, L.-W.; Paul Alivisatos, A. *Nature* **2004**, *430*, 190.

(9) Manna, L.; Milliron, D. J.; Meisel, A.; Scher, E. C.; Alivisatos, A. P. *Nat. Mater.* **2003**, *2*, 382.

(10) Johansson, J.; Bolinsson, J.; Ek, M.; Caroff, P.; Dick, K. A. *ACS Nano* **2012**, *6*, 6142.

(11) Spirkoska, D.; Arbiol, J.; Gustafsson, A.; Conesa-Boj, S.; Glas, F.; Zardo, I.; Heigoldt, M.; Gass, M. H.; Bleloch, A. L.; Estrade, S.; Kaniber, M.; Rossler, J.; Peiro, F.; Morante, J. R.; Abstreiter, G.; Samuelson, L.; Morral, A. F. I. *Phys. Rev. B* **2009**, *80*, 245325.

(12) Fiore, A.; Mastria, R.; Lupo, M. G.; Lanzani, G.; Giannini, C.; Carlino, E.; Morello, G.; De Giorgi, M.; Li, Y.; Cingolani, R.; Manna, L. *J. Am. Chem. Soc.* **2009**, *131*, 2274.

(13) Han, S. K.; Gong, M.; Yao, H. B.; Wang, Z. M.; Yu, S. H. *Angew. Chem., Int. Ed.* **2012**, *51*, 6365.

(14) Zhuang, T.-T.; Fan, F.-J.; Gong, M.; Yu, S.-H. *Chem. Commun.* **2012**, *48*, 9762.

(15) Zamani, R. R.; Ibanez, M.; Luysberg, M.; Garcia-Castello, N.; Houben, L.; Prades, J. D.; Grillo, V.; Dunin-Borkowski, R. E.; Morante, J. R.; Cabot, A.; Arbiol, J. *ACS Nano* **2014**, *8*, 2290.

(16) Wang, J. J.; Singh, A.; Liu, P.; Singh, S.; Coughlan, C.; Guo, Y. N.; Ryan, K. M. *J. Am. Chem. Soc.* **2013**, *135*, 7835.

(17) Brutchey, R. L. *Acc. Chem. Res.* **2015**, *48*, 2918.

(18) Fan, F. J.; Wu, L.; Gong, M.; Chen, S. Y.; Liu, G. Y.; Yao, H. B.; Liang, H. W.; Wang, Y. X.; Yu, S. H. *Sci. Rep.* **2012**, *2*, 952.

(19) Wu, L.; Fan, F.-J.; Gong, M.; Ge, J.; Yu, S.-H. *Nanoscale* **2014**, *6*, 3418.

(20) Singh, S.; Liu, P.; Singh, A.; Coughlan, C.; Wang, J. J.; Lusi, M.; Ryan, K. M. *Chem. Mater.* **2015**, *27*, 4742.

(21) Wang, J. J.; Liu, P.; Seaton, C. C.; Ryan, K. M. *J. Am. Chem. Soc.* **2014**, *136*, 7954.

(22) Ibáñez, M.; Zamani, R.; Li, W.; Cadavid, D.; Gorsse, S.; Katcho, N. A.; Shavel, A.; López, A. M.; Morante, J. R.; Arbiol, J.; Cabot, A. *Chem. Mater.* **2012**, *24*, 4615.

(23) Pan, D.; An, L.; Sun, Z.; Hou, W.; Yang, Y.; Yang, Z.; Lu, Y. *J. Am. Chem. Soc.* **2008**, *130*, 5620.

(24) Wang, J.-J.; Wang, Y.-Q.; Cao, F.-F.; Guo, Y.-G.; Wan, L.-J. *J. Am. Chem. Soc.* **2010**, *132*, 12218.

(25) Weil, B. D.; Connor, S. T.; Cui, Y. *J. Am. Chem. Soc.* **2010**, *132*, 6642.

(26) Guo, Q.; Kim, S. J.; Kar, M.; Shafarman, W. N.; Birkmire, R. W.; Stach, E. A.; Agrawal, R.; Hillhouse, H. W. *Nano Lett.* **2008**, *8*, 2982.

(27) Chen, S. Y.; Gong, X. G.; Walsh, A.; Wei, S. H. *Phys. Rev. B* **2009**, *79*, 165211.

(28) Fan, F.-J.; Wu, L.; Yu, S.-H. *Energy Environ. Sci.* **2014**, *7*, 190.

(29) Norako, M. E.; Franzman, M. A.; Brutchey, R. L. *Chem. Mater.* **2009**, *21*, 4299.

(30) Norako, M. E.; Brutchey, R. L. *Chem. Mater.* **2010**, *22*, 1613.

(31) Koo, B.; Patel, R. N.; Korgel, B. A. *J. Am. Chem. Soc.* **2009**, *131*, 3134.

(32) Kruszynska, M.; Borchert, H.; Parisi, J.; Kolny-Olesiak, J. *J. Am. Chem. Soc.* **2010**, *132*, 15976.

(33) Luo, J.; Tilley, S. D.; Steier, L.; Schreier, M.; Mayer, M. T.; Fan, H. J.; Gratzel, M. *Nano Lett.* **2015**, *15*, 1395.

(34) Zheng, L.; Xu, Y.; Song, Y.; Wu, C.; Zhang, M.; Xie, Y. *Inorg. Chem.* **2009**, *48*, 4003.

(35) Lei, S.; Wang, C.; Liu, L.; Guo, D.; Wang, C.; Tang, Q.; Cheng, B.; Xiao, Y.; Zhou, L. *Chem. Mater.* **2013**, *25*, 2991.

(36) Qi, Y.; Liu, Q.; Tang, K.; Liang, Z.; Ren, Z.; Liu, X. *J. Phys. Chem. C* **2009**, *113*, 3939.

(37) Wei, S.-H.; Zhang, S. B.; Zunger, A. *Phys. Rev. B* **1999**, *59*, R2478.

(38) Tang, A.; Hu, Z.; Yin, Z.; Ye, H.; Yang, C.; Teng, F. *Dalton Trans.* **2015**, *44*, 9251.

(39) Witt, E.; Kolny-Olesiak, J. *Chem. - Eur. J.* **2013**, *19*, 9746.

(40) Tang, J.; Hinds, S.; Kelley, S. O.; Sargent, E. H. *Chem. Mater.* **2008**, *20*, 6906.

(41) Fan, F.-J.; Wu, L.; Gong, M.; Liu, G.; Wang, Y.-X.; Yu, S.-H.; Chen, S.; Wang, L.-W.; Gong, X.-G. *ACS Nano* **2013**, *7*, 1454.

(42) Ibáñez, M.; Cadavid, D.; Zamani, R.; García-Castelló, N.; Izquierdo-Roca, V.; Li, W.; Fairbrother, A.; Prades, J. D.; Shavel, A.; Arbiol, J.; Pérez-Rodríguez, A.; Morante, J. R.; Cabot, A. *Chem. Mater.* **2012**, *24*, 562.

(43) Hsu, W. C.; Zhou, H.; Luo, S.; Song, T. B.; Hsieh, Y. T.; Duan, H. S.; Ye, S.; Yang, W.; Hsu, C. J.; Jiang, C.; Bob, B.; Yang, Y. *ACS Nano* **2014**, *8*, 9164.

(44) Winkler, M. T.; Wang, W.; Gunawan, O.; Hovel, H. J.; Todorov, T. K.; Mitzi, D. B. *Energy Environ. Sci.* **2014**, *7*, 1029.

(45) van Embden, J.; Chesman, A. S.; Della Gaspera, E.; Duffy, N. W.; Watkins, S. E.; Jasieniak, J. J. *J. Am. Chem. Soc.* **2014**, *136*, 5237.

(46) Chiang, M. Y.; Chang, S. H.; Chen, C. Y.; Yuan, F. W.; Tuan, H. Y. *J. Phys. Chem. C* **2011**, *115*, 1592.

(47) McDaniel, H.; Koposov, A. Y.; Draguta, S.; Makarov, N. S.; Pietryga, J. M.; Klimov, V. I. *J. Phys. Chem. C* **2014**, *118*, 16987.

(48) Meinardi, F.; McDaniel, H.; Carulli, F.; Colombo, A.; Velizhanin, K. A.; Makarov, N. S.; Simonutti, R.; Klimov, V. I.; Brovelli, S. *Nat. Nanotechnol.* **2015**, *10*, 878.

(49) Cheng, Y.; Jin, C.; Gao, F.; Wu, X.; Zhong, W.; Li, S.; Chu, P. K. *J. Appl. Phys.* **2009**, *106*, 123505.

DOI: 10.1021/jacs.5b13288
J. Am. Chem. Soc. 2016, 138, 5576−5584

(50) Tanino, H.; Maeda, T.; Fujikake, H.; Nakanishi, H.; Endo, S.; Irie, T. *Phys. Rev. B* **1992**, *45*, 13323.
(51) Guha, P.; Das, D.; Maity, A.; Ganguli, D.; Chaudhuri, S. *Sol. Energy Mater. Sol. Cells* **2003**, *80*, 115.
(52) Yang, C. C.; Li, S. *J. Phys. Chem. B* **2008**, *112*, 14193.
(53) Zeiri, L.; Patla, I.; Acharya, S.; Golan, Y.; Efrima, S. *J. Phys. Chem. C* **2007**, *111*, 11843.
(54) Singh, A.; Singh, S.; Levcenko, S.; Unold, T.; Laffir, F.; Ryan, K. M. *Angew. Chem., Int. Ed.* **2013**, *52*, 9120.
(55) Wu, X. J.; Huang, X.; Qi, X.; Li, H.; Li, B.; Zhang, H. *Angew. Chem., Int. Ed.* **2014**, *53*, 8929.
(56) Lei, S.; Sobhani, A.; Wen, F.; George, A.; Wang, Q.; Huang, Y.; Dong, P.; Li, B.; Najmaei, S.; Bellah, J.; Gupta, G.; Mohite, A. D.; Ge, L.; Lou, J.; Halas, N. J.; Vajtai, R.; Ajayan, P. *Adv. Mater.* **2014**, *26*, 7666.
(57) Chirilă, A.; Buecheler, S.; Pianezzi, F.; Bloesch, P.; Gretener, C.; Uhl, A. R.; Fella, C.; Kranz, L.; Perrenoud, J.; Seyrling, S.; et al. *Nat. Mater.* **2011**, *10*, 857.
(58) Chirilă, A.; Reinhard, P.; Pianezzi, F.; Bloesch, P.; Uhl, A. R.; Fella, C.; Kranz, L.; Keller, D.; Gretener, C.; Hagendorfer, H.; et al. *Nat. Mater.* **2013**, *12*, 1107.
(59) Chen, S. Y.; Walsh, A.; Luo, Y.; Yang, J. H.; Gong, X. G.; Wei, S. H. *Phys. Rev. B* **2010**, *82*, 195203.

DOI: 10.1021/jacs.5b13288
J. Am. Chem. Soc. 2016, 138, 5576−5584